Optica Applicata, Vol. XLVIII, No. 3, 2018
10.5277/oa180304

Focusing of linearly polarized helico-conical Lorentz beam with sine-azimuthal variation wavefront

YING BAO, JINGHENG LAN, YU MIAO, DAWEI ZHANG, XIUMIN GAO*

University of Shanghai for Science and Technology, Shanghai 200093, China

*Corresponding author: gxm@usst.edu.cn

In this article a theoretical research is described into focusing of a linearly polarized helico-conical Lorentz beam with a sine-azimuthal variation wavefront. The simulation results show the vortex charge on the axis, which has an obvious modulation effect on the focal modes of the Lorenz beam under certain beam parameters and phase parameters. Both the phase parameter and the vortex charge are zero, the focal spot appears round. The focal spot is symmetric about *y* axis when the charge is 0 and the phase parameter is adjusted. And the focal evolution patterns vary remarkably under different beam parameters and the phase parameters. In the process of focus evolution, there appears some novel focal patterns, such as a circle, a "T", a butterfly, a small running humanoid, a whale tail, a flower of four leaves, a serpentine, a goldfish, a Chinese knot and an octopus, which indicates that the focus mode of the optical vortex Lorentz beam can be altered by changing the phase parameters and vortex charge.

Keywords: Lorentz beam, focusing properties, optical vortex.

1. Introduction

In recent years, laser beams of different shapes have attracted great interest of optical workers because of their special applications, and the Lorenz beam is a case in point. As a realizable beam, the Lorenz beam is introduced by GAWHARY and SEVERINI [1–3]. On the one hand, due to the relatively big angle expansion of the Lorentz distribution [4], the Lorenz beam is suitable for describing some laser light sources with larger divergence, but Gaussian distribution is not suitable, instead, the Lorentz distribution is a relatively good approximation. On the other hand, the characterization of laser beams has always been a hot field in laser optics, and the beam quality has been extensively studied both in the paraxial approximation framework and in the nonparaxial range [5–8]. The beam transmission factor is suggested to represent the beam quality of the laser beam, and the beam transmission factor does play an important role in the characteriza-

tion of the beam quality of the laser beam [9, 10]. Recently, the study on Lorenz wavefront focusing sine linear polarization azimuth shows that the source model changes greatly on the basis of the beam parameters and phase parameters, and some new forms of focus patterns may appear, the focus mode of multiple peaks and the circular focus mode like a wheel [11].

The vortex beam by virtue of its complexity and considerable application prospect, has gradually become a hot research topic in academic circles in recent years, and it has been widely applied to the fields of the quantum encoding [12, 13], space optical communication [14, 15] and particle manipulation [16, 17]. The reason why the vortex beam is widely used especially in the field of optical manipulation is that the vortex beam with spiral wave can be focused into a ring of light trapping which is called the optical vortex [18–22]. To the best of our knowledge, however, there are no reported data on the focusing characteristics of optical vortices in Lorenz beams. In order to get insight into the focusing characteristics of Lorenz beams and to generalize their applications deeply, we investigate the focusing of linearly polarized helico-conical Lorentz beam with the sine-azimuthal variation wavefront. In Section 2, the principle of Lorenz beam focusing is described. The results are discussed in Section 3. And conclusions are summarized in Section 4.

2. Focusing linearly polarized helico-conical Lorentz beam with sine-azimuthal variation wavefront

In the investigated focusing system in this essay, the incident laser beam is chosen as the Lorenz beam, and the equation of pupil position of amplitude distribution of electric field in cylindrical coordinate system is below [1–3, 23–25],

$$E(r_0, \varphi) = A \frac{1}{\omega_x \omega_y} \frac{1}{1 + \cos^2(\varphi)(r_0/\omega_x)^2} \frac{1}{1 + \sin^2(\varphi)(r_0/\omega_y)^2} \tag{1}$$

where A is the constant, and the incident plane of the Lorentz beam is the product of two independent Lorenz functions. This article uses ω_x and ω_y as its parameters, where ω_x and ω_y are the parameters of the beam size, and r_0 is the radial coordinates, with A, ω_x, ω_y and $r_0 \in \Re$

$$\frac{r_0}{\omega_x} = \frac{\sin(\theta)}{\mathrm{NA}\, w_x}$$

where $w_x = \omega_x / r_\mathrm{p}$ is the relative beam of x coordinates, r_p is the outer radius of the optical aperture of the focusing system, and NA is the numerical aperture of the focusing system. It should be known that NA is defined as a product of the refractive index of the surrounding medium and the sinus of the aperture angle, namely NA = $n'\sin(\alpha)$,

where n' is the refractive index of a surrounding medium. The condition of the study is in the air, so $n' \approx 1$ and $\mathrm{NA} \approx \sin(\alpha)$. As a similar procedure,

$$\frac{r_0}{\omega_y} = \frac{\sin(\theta)}{\mathrm{NA}\, w_y}$$

where $w_y = \omega_y / r_\mathrm{p}$. It is important to note that the wavefront is the function of the azimuthal angle $\varphi = -\pi \sin(n\varphi)$, m is the vortex charge, K is a constant, and the value is 1.

To sum up, the Eq. (1) can be written as [26–30],

$$E(\theta, \varphi) = \frac{C}{w_x w_y} \frac{1}{1 + \left[\cos^2(\varphi)\sin^2(\theta)\right] / \left[\mathrm{NA}^2 w_x^2\right]} \frac{1}{1 + \left[\sin^2(\varphi)\sin^2(\theta)\right] / \left[\mathrm{NA}^2 w_y^2\right]} \times \exp\left[-i\pi \sin(n\varphi)\right] \exp\left[im\varphi\left(K - \frac{\sin(\theta)}{\mathrm{NA}}\right)\right] \tag{2}$$

In our study, the outer radius r_p of the optical aperture of the focusing system is constant, so $C = A / r_\mathrm{p}^2$ is also constant, and the n is the phase angle parameter, which represents the change frequency of the sinusoidal phase when the azimuth is increased. When the polarized light of the Lorenz beam is assumed to be along the x-axis, according to the vectorial diffraction theory, the electric field in the source region can be written as [31, 32],

$$\begin{aligned} \mathbf{E}(\rho, \psi, z) = \frac{1}{\lambda} \iint_{\Omega} \Big\{ & \left[\cos(\theta) + \sin^2(\varphi)(1 - \cos(\theta))\right]\mathbf{x} + \cos(\varphi)\sin(\varphi)\left[\cos(\theta) - 1\right]\mathbf{y} \\ & + \cos(\varphi)\sin(\theta)\mathbf{z} \Big\} \frac{C}{w_x w_y} \frac{1}{1 + \left[\cos^2(\varphi)\sin^2(\theta)\right] / \left[\mathrm{NA}^2 w_x^2\right]} \\ & \times \frac{1}{1 + \left[\sin^2(\varphi)\sin^2(\theta)\right] / \left[\mathrm{NA}^2 w_y^2\right]} \exp\left[-i\pi \sin(n\varphi)\right] \exp\left[im\varphi\left(K - \frac{\sin(\theta)}{\mathrm{NA}}\right)\right] \\ & \times \exp(im\varphi) \exp\left[-ik\rho \sin(\theta)\cos(\varphi - \psi)\right] \exp\left[-ikz\cos(\theta)\right] \sin(\theta)\, \mathrm{d}\theta\, \mathrm{d}\varphi \end{aligned} \tag{3}$$

The optical intensity in focal plane can be obtained calculated by the modulus square of Eq. (3), where $\varphi \in [0, 2\pi)$ and $\theta \in [0, \arcsin(\mathrm{NA})]$. Vector $\mathbf{x}$, $\mathbf{y}$ and $\mathbf{z}$ are unit vectors in the x, y, and z axes. Obviously, the incident light is depolarized and there

are three components (E_i, E_j, E_k) in X, Y, and Z, variable ρ, ψ, and z are the cylindrical coordinates of an observation point in the focal region.

3. Results and discussions

The intensity distributions are calculated and discussed here. It should be noted that the distance unit in all figures is the wavelength of an incident beam in vacuum. Since we are investigating the Lorenz beam, we observe the Lorentz beams with different w_x and w_y firstly. The wavefront modulation of Lorentz beams are all pure phase distribution, and their abstract modulus of pure phase distribution is 1, as shown in Fig. 1. When $w_x = w_y = 1$, the beam light intensity distribution is round, and the energy is strongest at the center, and the decreasing trend is gradually shown in the surrounding area, as shown in Fig. 1**a**. When $w_x = 1$, $w_y = 0.5$, the beam light intensity distribution is in a long shape and the energy is concentrated in the vicinity of $y = 0$, and the decreasing trend is still shown gradually in the surrounding area with the decrease of w_y, as shown in Fig. 1**b**. It can be seen that in the original Lorentz beam diagram, the size of w_x and w_y will affect the distribution of its beam strength. We will discuss the focusing properties further by fixing the numerical aperture NA below.

Here, the intensity distribution of the focal region is calculated as follows: NA = 0.95, $n = 0$, $w_x = w_y = 0.2$, $K = 1$, and at different m conditions, as shown in Fig. 2. It is obvious that the focal spot of the optical vortex has a great influence. When the charge on the axis of the optical vortex is increased, the focal spot is distorted from an ellipse to an irregular shape, and finally the center focal spot was replaced as a dark focal spot. In the case of $m = 0$, the entire focal spot is an elliptical point, as shown in Fig. 2**a**. When the topological charge is added, namely $m = 1$, the focal spot begins to distort, forming a vortex shape, as shown in Fig. 2**b**. When the vortex charge is increased, the weakness region increases and the vortex strengthens, as shown in Fig. 2**c**. When $m = 3$, the focal spot is complex and presents a dark focal spot in the center, and the focal spot is distributed around the center, which is the opposite of $m = 0$, as shown in Fig. 2**d**. Then, the phase parameter of 1, NA = 0.95, $n = 1$, $w_x = w_y = 0.2$, $K = 1$, and different m are also calculated and shown in Fig. 3. In the case of $m = 1$, the whole

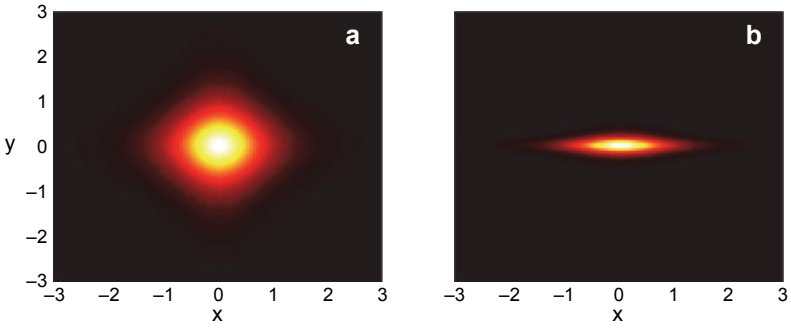

Fig. 1. Focal intensity distributions for $K = 1$, $n = 2$, $m = 3$ and $w_x = w_y = 1$ (**a**), $w_x = 1$, $w_y = 0.2$ (**b**).

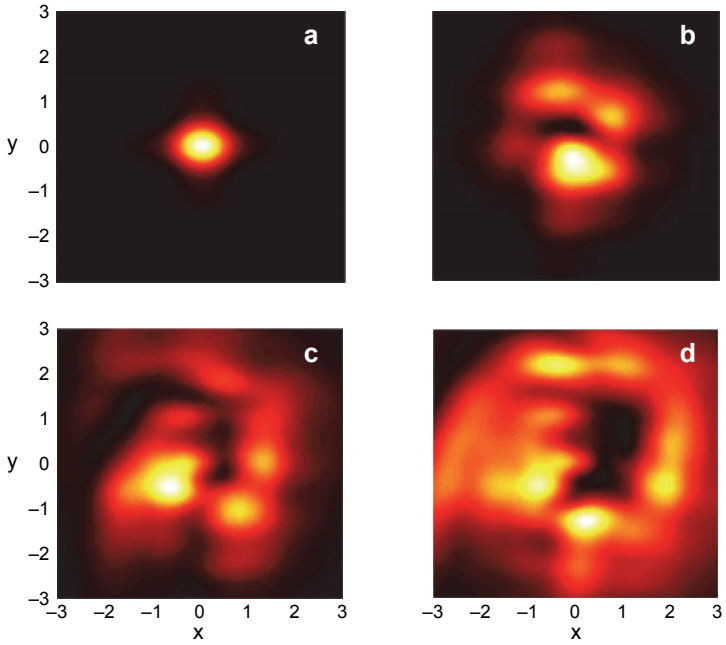

Fig. 2. Focal intensity distributions for NA = 0.95, $K = 1$, $n = 0$, $w_x = w_y = 0.2$ and $m = 0$ (**a**), $m = 1$ (**b**), $m = 2$ (**c**), $m = 3$ (**d**).

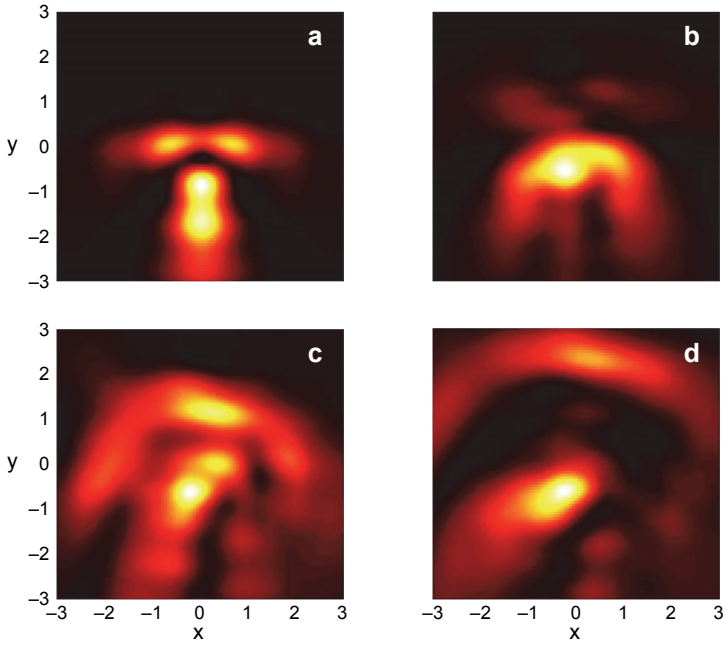

Fig. 3. Focal intensity distributions for NA = 0.95, $K = 1$, $n = 1$, $w_x = w_y = 0.2$ and $m = 0$ (**a**), $m = 1$ (**b**), $m = 2$ (**c**), $m = 3$ (**d**).

focal pattern turns on "T" shape, with one "∞" shape intensity branches and one rectangle intensity area, as shown in Fig. 3**a**. When $m = 1$, the "∞" shape region moves in the negative direction of the y-axis and evolves into a meniscus, as shown in Fig. 3**b**. When $m = 2$, the meniscus moves up to the right and is accompanied by two weak intensity spots besides, the column region moves along, and the weak intensity spots region spreads, as shown in Fig. 3**c**. Then the vortex charge increases, the meniscus and column region are separated, and the meniscus is strengthened into a ring, as shown in Fig. 3**d**.

Figure 4 illustrates the focal patterns under condition of NA = 0.95, $n = 2$, $w_x = w_y = 1$ and different charge. In the case of $m = 0$, there are two focal spots along the azimuth of 45 and 135 degrees, creating a weak intensity spot between each of the two focal spots, and a dark focal spot at the junction of the focal spot and the weak point, as shown in Fig. 4**a**. When an optical vortex is added to the shaft, namely, $m = 1$, the focal spot along the azimuth angle of 135 degrees direction with cracking, and interrupt the strong peak point of connection. Two of the corresponding intensity peak points are reduced to a weak intensity spot and shape into long bars, resulting in the shape of "butterfly", as shown in Fig. 4**b**. After increasing the vortex charges, the two types of weak intensity spot become intensity peaks, and the intensity peak at the left bottom was evolved into two weak intensity spots, showing the shape of "running man", as shown in Fig. 4**c**.

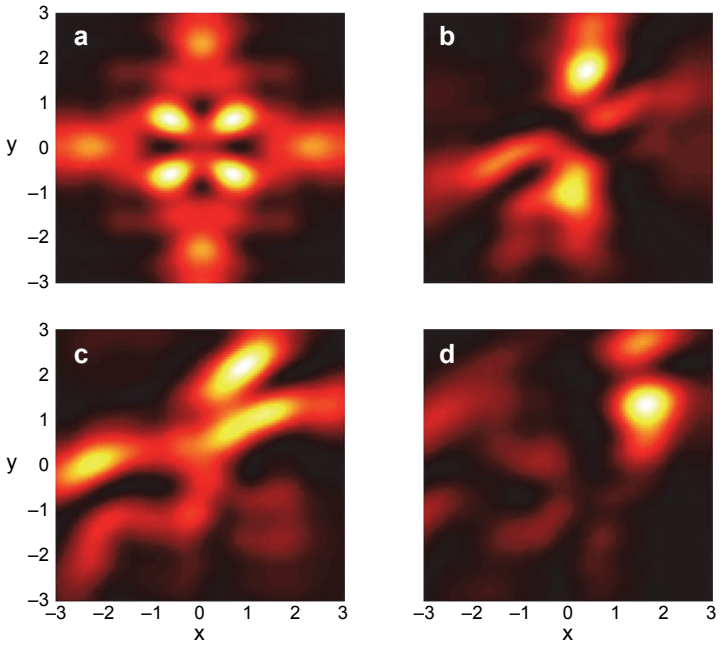

Fig. 4. Focal intensity distributions for NA = 0.95, $K = 1$, $n = 2$, $w_x = w_y = 0.2$ and $m = 0$ (**a**), $m = 1$ (**b**), $m = 2$ (**c**), $m = 3$ (**d**).

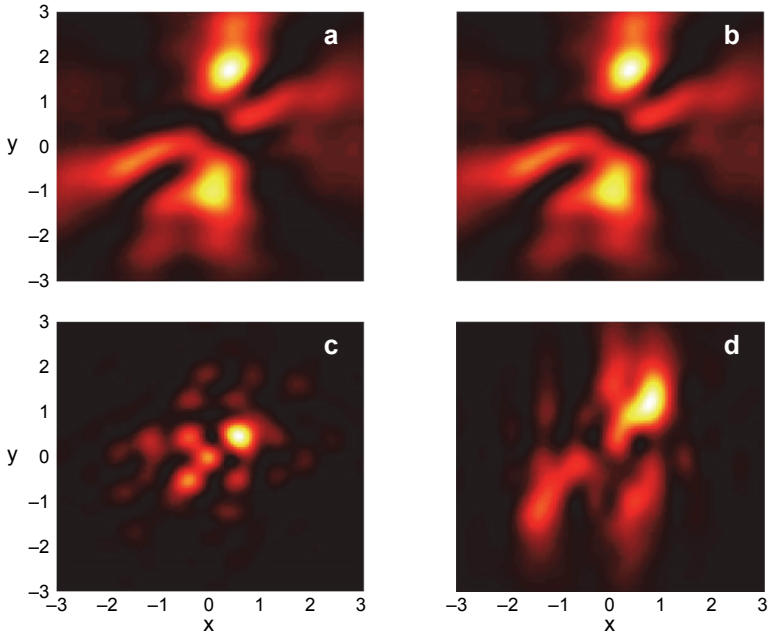

Fig. 5. Focal intensity distributions for NA = 0.95, $K = 1$, $n = 1$, $w_x = w_y = 0.2$, $m = 1$ and E (**a**), E_i (**b**), E_j (**c**), E_k (**d**).

However, as the charge increases to 3, a very obvious distortion occurs, the region of the intensity peaks shrinks into an ellipse, and the distribution of the weak intensity spots is extremely irregular, as shown in Fig. 4**d**. Here we add the intensity distributions of Lorentz beams with different w_x and w_y. The wavefront modulation of the Lorentz beams is a pure phase distribution, and the abstract modulus of pure phase distribution is 1. Now we consider the focal intensity distributions for different polarization components in the case of NA = 0.95, $K = 1$, $n = 2$, $w_x = w_y = 0.2$, $m = 1$ as shown in Fig. 5. Since Fig. 5**a** is in the situation of the combined action of three polarization components, Fig. 5**b** is for the condition of the polarization component E_i working, Fig. 5**c** is for the condition of the polarization component E_j working, and Fig. 5**d** illustrates that the focal intensity distributions is for the condition of the polarization component E_k working. It can be clearly seen that the polarization component E_i has the biggest influence on E.

Here, the phase parameter is chosen as 3, and focal patterns are given in Fig. 6 under condition of NA = 0.95, $n = 3$, $w_x = w_y = 0.2$, and different m. We can see that the focus mode becomes more complex than all cases above, and the distortion becomes more serious as the charge increases. In the case of $m = 0$, the whole focal pattern turns up in a whale tail shape, with a strength branch extending over a syncline and a crown shaped strength zone on both sides and one cylindrical region in the same direction as

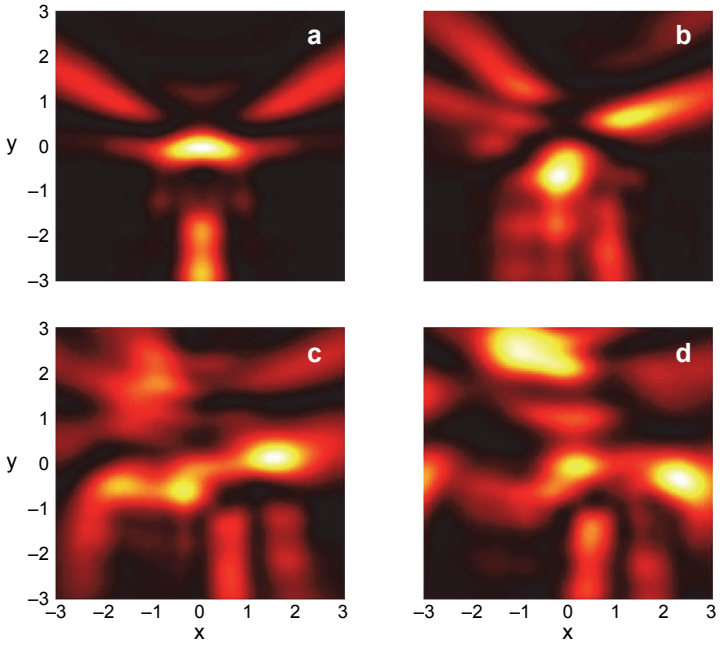

Fig. 6. Focal intensity distributions for NA = 0.95, $K = 1$, $n = 3$, $w_x = w_y = 0.2$ and $m = 0$ (**a**), $m = 1$ (**b**), $m = 2$ (**c**), $m = 3$ (**d**).

the y-axis, as shown in Fig. 6**a**. When $m = 1$, the two intensity branches begin to tilt to the upper right, and the crown and column strength regions begin to split, as shown in Fig. 6**b**. When $m = 2$, the two intensity branches begin to fuse, produce an "X" shape and move to the left, where the intermediate coronal region is transversely divided into bars, and the entire focal mode is irregularly distributed, as shown in Fig. 6**c**. After increasing the charge, the focal spot of the two intensity fusion parts increases, and the limb fracture occurs. At the same time, the strip region also breaks, as shown in Fig. 6**d**.

Figure 7 shows the focal intensity distributions for NA = 0.95, $n = 4$, $w_x = w_y = 0.2$ and different charge m. It can be seen that, compared to Figs. 7 and 3, the change of the total focal mode is very sharp at high phase parameters. When $m = 0$, there is an intensity peak at the mid-point, close to the four pavilion shape of a weak intensity spot, in direction respectively along the x-axis and y-axis there is a dark focal spot between the intensity peak and four weak intensity spots, namely four shaped flowers. At the same time, there are two long lines of weak intensity spots between each two petals, as shown in Fig. 7**a**. When the vortex charge is added to the axis, the intensity peak in the middle is shifted, and the shape of the petals is distorted into a long strip. At the same time, it changes to an intensity peak and presents a "firework shape", as shown in Fig. 7**b**. After further increasing the vortex charge, the focal spot rotates in a clockwise direction, and the separation becomes more serious. At $m = 3$, there are only two

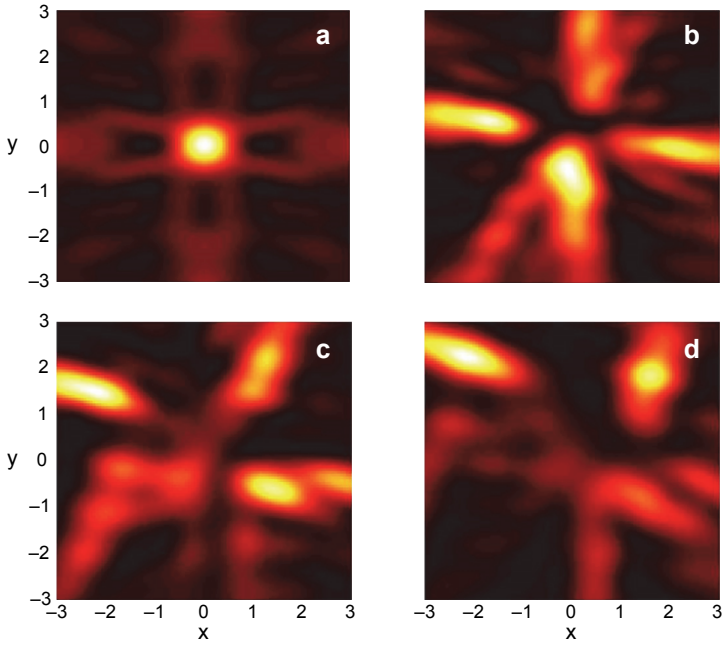

Fig. 7. Focal intensity distributions for NA = 0.95, $K = 1$, $n = 4$, $w_x = w_y = 0.2$ and $m = 0$ (**a**), $m = 1$ (**b**), $m = 2$ (**c**), $m = 3$ (**d**),.

intensity separated peaks, and they are accompanied by an irregular distribution of weak intensity spots, as shown in Fig. 7**d**.

Based on the discussion above, the change in the value of w_x from 0.2 to 1, and corresponding intensity distributions are shown in Fig. 8. By comparing Fig. 8 with Fig. 2, it can be seen that the beam parameter w_x has a considerable influence on the focal spot, and the evolution of the focal spot is different as the charge increases. When $m = 0$, both images are rounded, as shown in Fig. 8**a**. When $m = 1$, there is an annular weak intensity spot on the left of the focal spot, as shown in Fig. 8**b**. When the charge increases from 1 to 2, the focal spot assumes a serpentine distribution. For larger m, the snake tail splits in the image and a large annular weak intensity spot appears on the left, as shown in Fig. 8**d**. And we can see that in the same evolutionary process, the intensity peak of Fig. 7 is moving along the x-axis, and the center diffuses into the surrounding direction in Fig. 1. Now, the value of the phase parameter is adjusted up to 2, focal intensity distributions for NA = 0.95, $n = 2$, $w_x = 1$, $w_y = 0.2$, and different m are shown in Fig. 9. When $m = 0$, the two love-shaped focal spots are mirror symmetrical and are connected with the middle dark focal spot to form a bidirectional arrow shape, as shown in Fig. 9**a**. When $m = 1$, there are two love-shaped focal spots at fixed point position, the rest of the spin on the right, and one of the focal spots becomes weak and splits. The whole appears as a goldfish shape, as shown in Fig. 9**b**. When $m = 2$, the

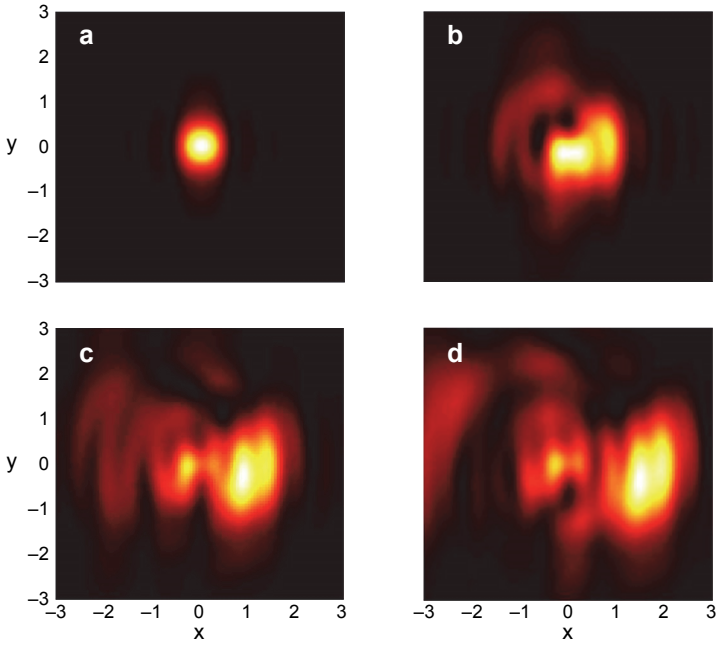

Fig. 8. Focal intensity distributions for NA = 0.95, $K = 1$, $n = 0$, $w_x = 1$, $w_y = 0.2$ and $m = 0$ (**a**), $m = 1$ (**b**), $m = 2$ (**c**), $m = 3$ (**d**).

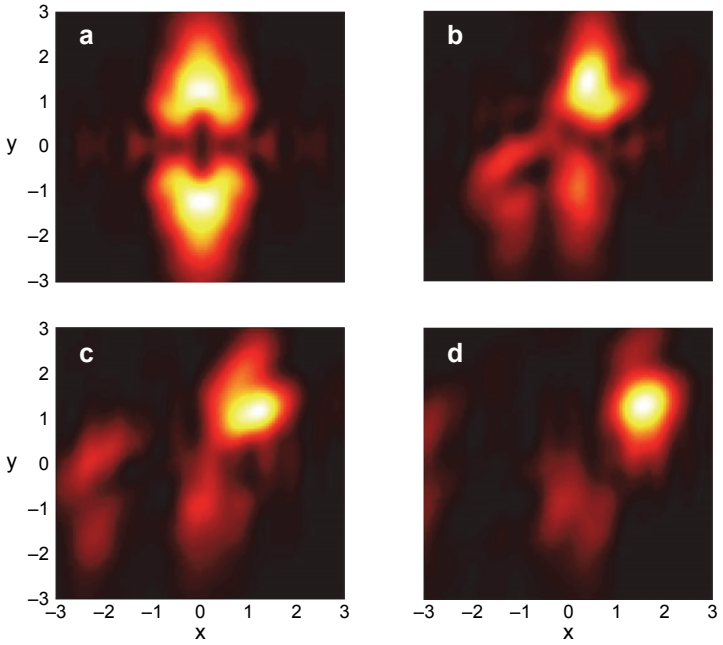

Fig. 9. Focal intensity distributions for NA = 0.95, $K = 1$, $n = 2$, $w_x = 1$, $w_y = 0.2$ and $m = 0$ (**a**), $m = 1$ (**b**), $m = 2$ (**c**), $m = 3$ (**d**).

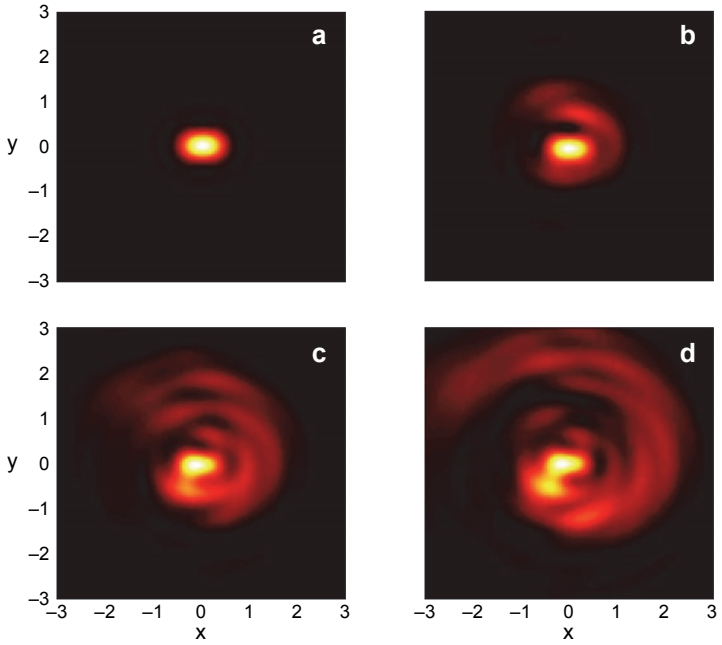

Fig. 10. Focal intensity distributions for NA = 0.95, $K = 1$, $n = 0$, $w_x = w_y = 1$ and $m = 0$ (**a**), $m = 1$ (**b**), $m = 2$ (**c**), $m = 3$ (**d**).

tail of the goldfish shaped focal spot is further divided, as shown in Fig. 9**c**. When the charge gets up to 3, the focal pattern shrinks into one elliptic shape with a weak intensity spot in the lower left corner, as shown in Fig. 9**d**.

Now we change the value of w_y from 0.2 to 1, and corresponding the intensity distributions are shown in Fig. 10. By comparing Fig. 10 with Fig. 2, it can be seen that the effect of the change of w_x and w_y on the focal pattern evolution is very considerable, and the evolution of the focal spot after adding the charge has a certain regularity. By comparing Fig. 10 with Fig. 9, the higher w_y makes the whole focal pattern change smaller. In Fig. 9, the focal spot position is still almost in the center, and there is no offset along the x-axis direction. As far as the weak intensity spot is concerned, when $w_y = 0.2$ is present, as the charge increases, the weak intensity spot appears more irregular, as shown in Fig. 8. But in Fig. 10, $w_y = 1$, the vortex shape of the weak spot increases as the charge increases, showing a relatively regular pattern.

Figure 11 shows the focal intensity distributions for NA = 0.95, $n = 2$, $w_x = w_y = 1$, and different m. When $m = 0$, the full focal mode exhibits a Chinese junction shape, as shown in Fig. 11**a**. When $m = 1$, the focal spot begins to turn along the azimuth of 45 degrees and is accompanied by a narrowing of the fusion splitting phenomenon, as shown in Fig. 11**b**. When the charge on the count of 2 is increased, the strong peak point is dotted into elliptical directions along the 45 degrees azimuth direction, the weak intensity spot turns into the strip "feet", full focus mode shows "octopus" shape, with the ring "ripple" weak intensity spots besides, as shown in Fig. 11**c**. When $m = 3$, the

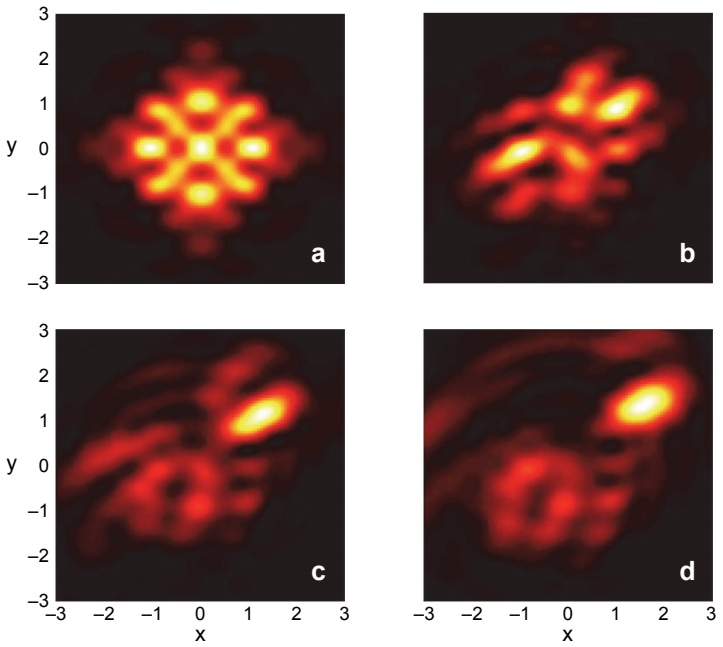

Fig. 11. Focal intensity distributions for NA = 0.95, $K = 1$, $n = 2$, $w_x = w_y = 1$ and $m = 0$ (**a**), $m = 1$ (**b**), $m = 2$ (**c**), $m = 3$ (**d**).

"foot" weak intensity spots begin to weaken, and the ring "ripple" weak intensity spots spread, as shown in Fig. 11**d**. The effect of charge on the focusing mode is still very impressive.

4. Conclusions

Focal spot intensity distribution plays an extremely important role in many optical systems. Since the beam is an electromagnetic field with a distinct direction of light propagation, most of the field energy is concentrated near the optical axis during propagation. Therefore, considering the axial vortex charge, eccentric shaft and other parameters, the beam parameters, and this article does research into the focusing of linearly polarized helico-conical Lorentz beam with sine-azimuthal variation wavefront. The results show that the vortex charge on the axis has an obvious modulation effect on the focal modes of the Lorenz beam under certain beam parameters and phase parameters. When both the phase parameter and the vortex charge are 0, and when the charge is 0 and the phase parameter is changed, the focal spot is symmetrical with respect to the y-axis. And the focal evolution patterns vary remarkably under different beam parameters and the phase parameters. In the process of focus evolution, there appears some novel focal patterns, such as a circle, a "T", a butterfly, a small running

humanoid, a whale tail, a flower of four leaves, a serpentine, a goldfish, a Chinese knot and an octopus. Therefore, it can be concluded that the optical vortex Lorentz beam can change the focus mode by means of changing the phase parameters and the vortex charge on the axis, which contributes to extending the application of Lorentz beam in some focusing systems.

Although focusing properties of beams have been investigated in this manuscript, the experiment research method should be noted. In fact, we are constructing a system for experimental investigation. Spatial light modulator [33–35] can be used to obtain this kind of beams. Pure phase spatial light modulator can alter wavefront phase distribution, and a pure amplitude spatial light modulator can adjust wavefront amplitude distribution. Therefore, in the proposed optical system, two spatial light modulators are considered. Focusing properties of the novel kind of beams play an important role in many optical systems, and results shown in this manuscript may find wide applications in optical tweezers [36, 37], multiple point microscope [38], and optical machining. Tunable focal pattern may be used to construct dynamic optical tweezers.

Acknowledgements – This work was supported by the National Key Research and Development Plan "Earth Observation and Navigation" key special project (2017YFB0503100).

References

[1] El Gawhary O., Severini S., *Lorentz beams and symmetry properties in paraxial optics*, Journal of Optics A: Pure and Applied Optics 8(5), 2006, pp. 409–414.

[2] El Gawhary O., Severini S., *Lorentz beams as a basis for a new class of rentangularly symmetric optical fields*, Optics Communications 269(2), 2007, pp. 274–284.

[3] Torre A., Evans W.A.B., El Gawhary O., Severini S., *Relativistic Hermite polynomials and Lorentz beams*, Journal of Optics A: Pure and Applied Optics 10(11), 2008, article ID 115007.

[4] Naqwi A., Durst F., *Focusing of diode laser beams: a simple mathematical model*, Applied Optics 29(12), 1990, pp. 1780–1785.

[5] Dumke W.P., *The angular beam divergence in double-heterojunction lasers with very thin active regions*, IEEE Journal of Quantum Electronics 11(7), 1975, pp. 400–402.

[6] Lu Qunying, Chen Tingting, Ding Guilin, Yuan Xiao, *Propagation properties of Lorentz beam passing through first-order axisymmertric optical systems*, Chinese Journal of Lasers **35**(4), 2008, pp. 539–543.

[7] Guoquan Zhou, Jun Zheng, Yiqin Xu, *Investigation in the far field characteristics of Lorentz beam from the vectorial structure*, Journal of Modern Optics 55(6), 2008, pp. 993–1002.

[8] Zhou Guo-Quan, *Study on the propagation properties of Lorentz beam*, Acta Physica Sinica 57(6), 2008, pp. 3494–3498.

[9] Juguan Gu, Daomu Zhao, *Propagation characteristics of Gaussian beams through a paraxial ABCD optical system with an annular aperture*, Journal of Modern Optics 52(8), 2005, pp. 1065–1072.

[10] Goodman J.W., *Introduction to Fourier Optics*, McGraw-Hill, New York, 1968.

[11] Xiumin Gao, Dawei Zhang, Mei Ting, Fu Rui, Qiufang Zhan, Songlin Zhuang, *Focus shaping of linearly polarized Lorentz beam with sine-azimuthal variation wavefront*, Optik – International Journal for Light and Electron Optics 124(15), 2013, pp. 2079–2084.

[12] MAIR A., VAZIRI A., WEIHS G., ZEILINGER A., *Entanglement of the orbital angular-momentum states of photons*, Nature 412(6844), 2001, pp. 313–316.
[13] KRENN M., HANDSTEINER J., FINK M., FICKLER R., ZEILINGER A., *Twisted photon entanglement through turbulent air across Vienna*, PNAS 112(46), 2015, pp. 14197–14201.
[14] PATERSON C., *Atmospheric turbulence and orbital angular momentum of single photons for optical communication*, Physical Review Letters 94(15), 2005, article ID 153901.
[15] WILLNER A.E., HUANG H., YAN Y., REN Y., AHMED N., XIE G., BAO C., LI L., CAO Y., ZHAO Z., WANG J., LAVERY M.P.J., TUR M., RAMACHANDRAN S., MOLISCH A.F., ASHRAFI N., ASHRAFI S., *Optical communications using orbital angular momentum beams*, Advances in Optics and Photonics 7(1), 2015, pp. 66–106.
[16] LEE W.M., YUAN X.-C., CHEONG W.C., *Optical vortex beam shaping by use of highly efficient irregular spiral phase plates for optical micromanipulation*, Optics Letters 29(15), 2004, pp. 1796–1798.
[17] LIANG Y., YAO B., MA B., *et al.*, *Holographic optical trapping and manipulation based on phase-only liquid-crystal spatial light modulator*, Acta Physica Sinica **36**(3), 2016, article ID 0309001.
[18] GUTTINGER W., EIKEMEIER H., [Eds.], *Structure Stability in Physics*, Springer, Berlin, 1978, pp. 141–254.
[19] VASNETSOV M.V., STALIUNAS K., [Eds.], *Optical Vortices*, Nova Science Publishers, New York, 1999.
[20] KIVSHAR Y.S., PELINOVSKY D.E., *Self-focusing and transverse instabilities of solitary waves*, Physics Reports 331(4), 2000, pp. 117–195.
[21] ALLEN L., PADGETT M.J., BABIKER M., *IV The Orbital Angular Momentum of Light*, [In] *Progress in Optics*, Vol. 39, Elsevier, 1999, pp. 291–372.
[22] BARNETT S.M., ALLEN L., *Orbital angular momentum and nonparaxial light beams*, Optics Communications 110(5–6), 1994, pp. 670–678.
[23] GUOQUAN ZHOU, *The beam propagation factors and the kurtosis parameters of a Lorentz beam*, Optics and Laser Technology 41(8), 2009, pp. 953–955.
[24] ZHOU GUO-QUAN, *Fractional Fourier transform of Lorentz beams*, Chinese Physics B **18**(7), 2009, pp. 2779–2784.
[25] GUOQUAN ZHOU, *Generalized M^2 factors of truncated partially coherent Lorentz and Lorentz–Gauss beams*, Journal of Optics 12(1), 2010, article ID 015701.
[26] YU MIAO, GUANXUE WANG, XIANGYU ZENG, GUORONG SUI, RONGFU ZHANG, QIUFANG ZHAN, *Focusing properties of radially polarized helico-conical Lorentz–Gauss beam*, Optik – International Journal for Light and Electron Optics 136, 2017, pp. 289–294.
[27] FU RUI, DAWEI ZHANG, MEI TING, XIUMIN GAO, SONGLIN ZHUANG, *Focusing of linearly polarized Lorentz–Gauss beam with one optical vortex*, Optik – International Journal for Light and Electron Optics 124(17), 2013, pp. 2969–2973.
[28] XUN WANG, ZHIRONG LIU, DAOMU ZHAO, *Nonparaxial propagation of Lorentz–Gauss beams in uniaxial crystal orthogonal to the optical axis*, Journal of the Optical Society of America A 31(4), 2014, pp. 872–878.
[29] NEMOTO S., *Experimental evaluation of a new expression for the far field of a diode laser beam*, Applied Optics 33(27), 1994, pp. 6387–6392.
[30] HAIDONG WANG, XIUMIN GAO, XINMIAO LU, BOLUN LI, GAORAN QIAN, *Focusing properties of Lorentz –Gaussian beam with trigonometric function modulation*, Optik – International Journal for Light and Electron Optics 127(20), 2016, pp. 9436–9443.
[31] GU M., *Advanced Optical Imaging Theory*, Springer, Heidelberg, 2000.
[32] DJENAN GANIC, XIAOSONG GAN, MIN GU, *Focusing of doughnut laser beams by a high numerical -aperture objective in free space*, Optics Express 11(21), 2003, pp. 2747–2752.
[33] ZINCHIK A.A., *Application of spatial light modulators for generation of laser beams with a spiral phase distribution*, Scientific and Technical Journal of Information Technologies, Mechanics and Optics 15(5), 2015, pp. 817–824.
[34] ZHAOMIN TONG, XUYUAN CHEN, *Speckle reduction by angle diversity using a translucent spatial light modulator*, Optica Applicata 42(3), 2012, pp. 651–658.

[35] KOLOBRODOV V.G., TYMCHYK G.S., MYKYTENKO V.I., KOLOBRODOV M.S., *Physical and mathematical model of the digital coherent optical spectrum analyzer*, Optica Applicata 47(2), 2017, pp. 273–282.
[36] BERG-SØRENSEN K., FLYVBJERG H., *Power spectrum analysis for optical tweezers*, Review of Scientific Instruments 75(3), 2004, pp. 594–612.
[37] DROBCZYŃSKI S., DUŚ-SZACHNIEWICZ K., SYMONOWICZ K., GŁOGOCKA D., *Spectral analysis by a video camera in a holographic optical tweezers setup*, Optica Applicata 43(4), 2013, pp. 739–746.
[38] HAEBERLÉ O., XU C., DIETERLEN A., JACQUEY S., *Multiple-objective microscopy with three-dimensional resolution near 100 nm and a long working distance*, Optics Letters 26(21), 2001, pp. 1684–1686.

Received October 9, 2017
in revised form December 23, 2017